

## Deep CNN Model for Multimodal Medical Image Denoising

Walid El-Shafai<sup>1,2</sup>, Amira A. Mahmoud<sup>1</sup>, Anas M. Ali<sup>1,3</sup>, El-Sayed M. El-Rabaie<sup>1</sup>, Taha E. Taha<sup>1</sup>, Osama F. Zahran<sup>1</sup>, Adel S. El-Fishawy<sup>1</sup>, Naglaa F. Soliman<sup>4</sup>, Amel A. Alhussan<sup>5,\*</sup> and Fathi E. Abd El-Samie<sup>1</sup>

<sup>1</sup>Department Electronics and Electrical Communications, Faculty of Electronic Engineering, Menoufia University, Menouf, 32952, Egypt

<sup>2</sup>Security Engineering Laboratory, Department of Computer Science, Prince Sultan University, Riyadh, 11586, Saudi Arabia

<sup>3</sup>Alexandria Higher Institute of Engineering & Technology (AIET), Alexandria, Egypt

<sup>4</sup>Department of Information Technology, College of Computer and Information Sciences, Princess Nourah bint Abdulrahman University, Riyadh, 11671, Saudi Arabia

<sup>5</sup>Department of Computer Sciences, College of Computer and Information Sciences, Princess Nourah bint Abdulrahman University, Riyadh, Saudi Arabia

\*Corresponding Author: Amel A. Alhussan. Email: aaalhussan@pnu.edu.sa

Received: 25 February 2022; Accepted: 30 March 2022

**Abstract:** In the literature, numerous techniques have been employed to decrease noise in medical image modalities, including X-Ray (XR), Ultrasonic (Us), Computed Tomography (CT), Magnetic Resonance Imaging (MRI), and Positron Emission Tomography (PET). These techniques are organized into two main classes: the Multiple Image (MI) and the Single Image (SI) techniques. In the MI techniques, images usually obtained for the same area scanned from different points of view are used. A single image is used in the entire procedure in the SI techniques. SI denoising techniques can be carried out both in a transform or spatial domain. This paper is concerned with single-image noise reduction techniques because we deal with single medical images. The most well-known spatial domain noise reduction techniques, including Gaussian filter, Kuan filter, Frost filter, Lee filter, Gabor filter, Median filter, Homomorphic filter, Speckle reducing anisotropic diffusion (SRAD), Nonlocal-Means (NL-Means), and Total Variation (TV), are studied. Also, the transform domain noise reduction techniques, including wavelet-based and Curvelet-based techniques, and some hybridization techniques are investigated. Finally, a deep (Convolutional Neural Network) CNN-based denoising model is proposed to eliminate Gaussian and Speckle noises in different medical image modalities. This model utilizes the Batch Normalization (BN) and the ReLU as a basic structure. As a result, it attained a considerable improvement over the traditional techniques. The previously mentioned techniques are evaluated and compared by calculating qualitative visual inspection and quantitative parameters like Peak Signal-to-Noise Ratio (PSNR), Correlation Coefficient ( $C_r$ ), and system complexity to determine the optimum denoising algorithm to be applied universally. Based on the quality metrics, it is demonstrated that the proposed deep CNN-based denoising



This work is licensed under a Creative Commons Attribution 4.0 International License, which permits unrestricted use, distribution, and reproduction in any medium, provided the original work is properly cited.

model is efficient and has superior denoising performance over the traditional denoising techniques.

**Keywords:** Image enhancement; medical imaging; speckle noise; Gaussian noise; denoising filters; CNN denoising

## 1 Introduction

Medical scans are great tools that help specialists to identify the different abnormalities in the body organs. These scans can detect, diagnose, and treat different diseases. The main used medical scans are Us, XR, CT, PET, and MRI [1–3]. Unfortunately, Us images suffer from the speckle noise [4–6], resulting from destructive interference between the reflected echoes. X-ray, CT, PET, and MRI imaging systems are sometimes pervaded by Gaussian noise [7], which is a statistical artifact. It arises mainly from sensor noise, heat, propagation, or circuit noise. In the literature work [8,9], frame and traditional models have been studied to enhance the quality of different image modalities. Noise removal techniques are a preprocessing stage commonly used in computer vision, such as classification, recording, segmentation, and reconstruction image. Therefore, traditional techniques are used to remove noise from medical images [10].

As shown in Fig. 1, we have selected some well-known noise reduction techniques. The first group is the spatial domain techniques, including the Gaussian filter [11], which is simple to implement but loses a few image details. Gabor filter [12] cannot remove image noise, especially at high noise levels. Lee filter [13,14] is a well-known adaptive local filter that takes the mean of neighborhood pixels for denoising and preserves the edges and other image details, but it is disliked because it eliminates the noise nearest area of edges. Frost filter [15] uses an exponential kernel. It reduces the image noise, but it smooths the image and takes more computation time. Kuan filter [16] is better than the Lee filter in eliminating noise and preserving the edges nearest the boundaries of the images, but its parameters need to be determined properly.

Median filter [16,17] is a non-linear filter, whose method is based on the median pixel value of its nearby neighbors, sustains the edge. However, in the case of speckle noise, it results in blurred images or reduced information in the edge [18]. Homomorphic filter [19,20] gradually reduces noise and improves the image contrast. SRAD [21,22] can effectively reduce noise and preserve image edges, but its performance degrades at high noise variances. The restored pixel value NL-Means filter [23] depends on the weighted average of surrounding pixels. It gives good denoising performance. The TV technique [24] is based on the principle that images with excessive features have huge total variation, So, it eliminates the noise while sustaining important features such as edges. The other group is the transform domain noise reduction techniques, including wavelet-based [25] techniques and curvelet-based techniques. Weiner filter [26] based on wavelet transform is efficient to remove noise from the image, smooth the image, and sustain the edges but partly removes noise from the bright region and reduces the brightness of the image.

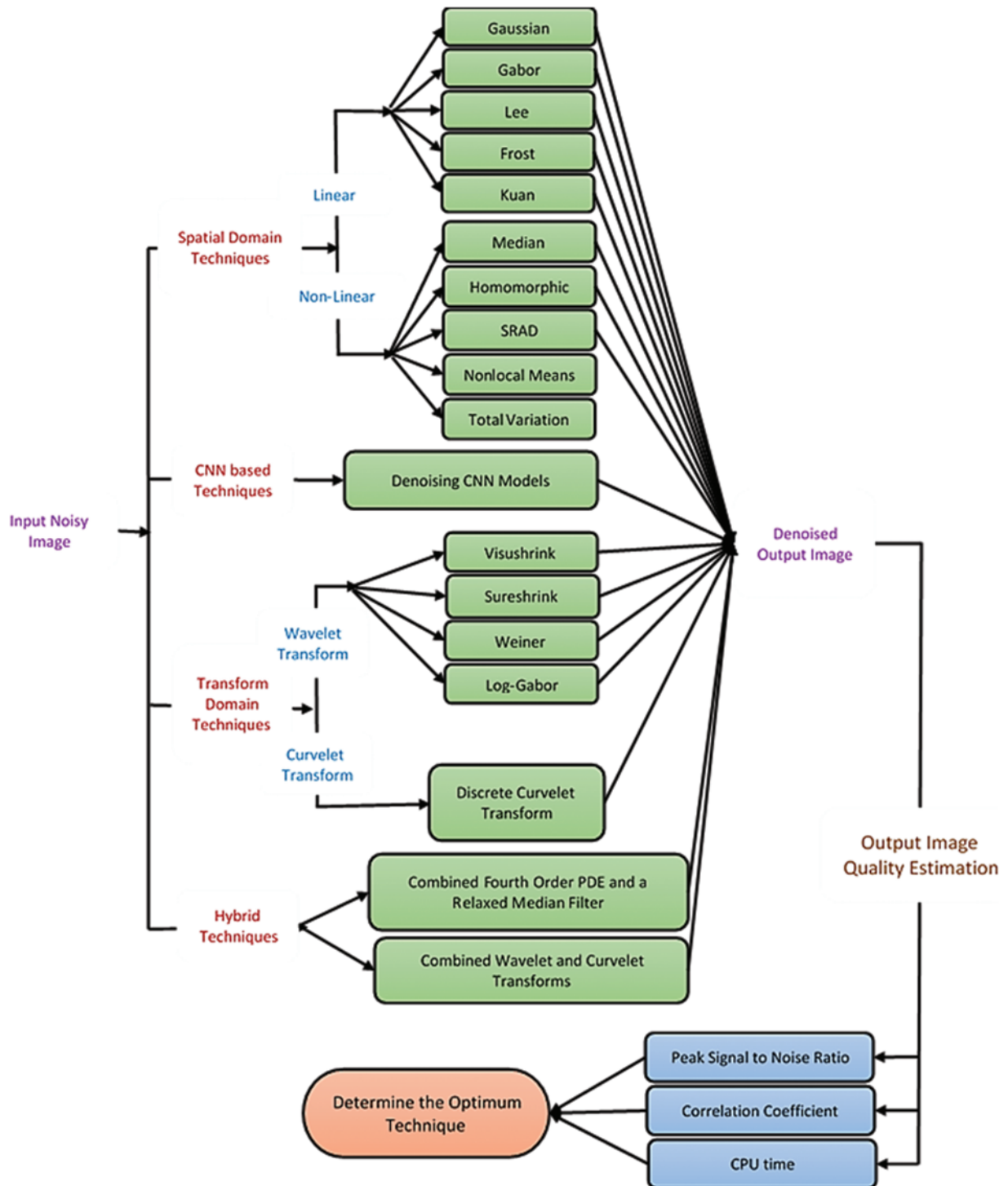


Figure 1: The main goal and motivation of the work

The Log-Gabor filter [27] is particularly useful in image denoising because it can better capture the features of the image. On the other hand, curvelet-based techniques are most acceptable for image denoising as they present the image edges [28]. There are some hybridization techniques as the combined fourth-order PDE and a relaxed median filter algorithm (Hybrid1) [29] and the combined Wavelet and Curvelet Transform Algorithm (Hybrid2) [30]. Finally, a proposed CNN-based denoising model is proposed to eliminate Speckle and Gaussian noise in different modalities of medical images. The denoising CNN achieved a significant performance improvement over conventional techniques in image denoising using convolution, BN, and ReLU as a basic structure. We evaluated and compared these techniques by calculating qualitative visual inspection and quantitative parameters like PSNR,  $C_r$ , and system complexity [31]. As a result, we can suggest the best technique that suits each imaging modality and the features of the denoised medical images. Therefore, we can determine an optimum denoising algorithm to be applied universally.

The major impacts of this research work are:

- Presenting a comparative analysis of traditional medical image denoising techniques and the proposed CNN-based denoising model for multi-modal images.
- It is found that the denoising CNN model has a superior performance in contrast to other denoising models.
- The denoising CNN can easily handle different medical images with different characteristics and different noise types. Therefore, the CNN-based denoising model can improve performance more than other models for various noise levels.

The rest of this paper is arranged as follows. Section 2 reviews the medical image noise reduction techniques. Section 3 illustrates the suggested CNN-based noise reduction model. Section 4 analyses the outcomes and discusses the obtained various results. Section 5 shows the concluding remarks.

## 2 Medical Image Noise Reduction Techniques

In this paper, we are concerned with single image noise reduction techniques. Single-image noise reduction techniques can be carried out in the spatial or transform domains [5,10].

### 2.1 Spatial Domain-Based Noise Reduction Techniques

#### 2.1.1 Linear Filtering Techniques

- **Gaussian Filter**

It has an impulse response which is a Gaussian function. It can be represented as [11]:

$$f(x, y) = \sqrt{\frac{1}{4\pi\sigma^2}} e^{-(x^2+y^2)/2\sigma^2} \quad (1)$$

- **Gabor Filter**

The impulse response of the Gabor filter [12] is specified by a sinusoidal function multiplied by a Gaussian kernel. It includes real and imaginary parts illustrating perpendicular directions. These two parts may be arranged into a complex number or employed separately.

The complex form is given by:

$$g(x, y; \lambda, \theta, \sigma, \gamma) = \exp\left(-\frac{x^2 + \gamma^2 y^2}{2\sigma^2}\right) \exp\left(i\left(2\pi \frac{x'}{\lambda} + \psi\right)\right) \tag{2}$$

The real is:

$$g(x, y; \lambda, \theta, \sigma, \gamma) = \exp\left(-\frac{x^2 + \gamma^2 y^2}{2\sigma^2}\right) \cos\left(2\pi \frac{x'}{\lambda} + \psi\right) \tag{3}$$

The imaginary is:

$$g(x, y; \lambda, \theta, \sigma, \gamma) = \exp\left(-\frac{x^2 + \gamma^2 y^2}{2\sigma^2}\right) \sin\left(2\pi \frac{x'}{\lambda} + \psi\right) \tag{4}$$

where  $x' = x \cos \theta + y \sin \theta$  and  $y' = -x \sin \theta + y \cos \theta$

• **Lee Filter**

It is based on the idea that the filtering will be carried out if the variance in a specific region is low or uniform [13,14]. Apart from that, filtering will not be implemented. Let  $\mathbf{I}$  be an image pixel corrupted by noise  $n$ ; the lee filter has the general form:

$$\hat{\mathbf{I}} = \bar{\mathbf{I}}_n + [\mathbf{I}_n - \bar{\mathbf{I}}_n] w_l \tag{5}$$

where  $w_l$  is the weighting function for Lee filter ranging between 0 for uniform regions and 1 for non-uniform regions,  $\bar{\mathbf{I}}_n$  is the mean of pixels in a moving window,  $\mathbf{I}_n$  is the noisy image, and  $\hat{\mathbf{I}}$  is the output image.

• **Frost Filter**

It is an adaptive filter suitable for noise reduction [15,16]. It acts as a mean filter in smooth or uniform regions and a high-pass filter in non-uniform regions. The Frost filter is formed as:

$$\hat{\mathbf{I}} = \frac{\mathbf{I}_{n1}M_1 + \mathbf{I}_{n2}M_2 + \dots + \mathbf{I}_{nn}M_n}{M_1 + M_2 + \dots + M_n} \tag{6}$$

where  $M$  is the exponential weighting factor.

• **Kuan Filter**

It is similar to the Lee filter but with various weighting functions [14,15]. It is computed in the same way as the Lee filter:

$$\hat{\mathbf{I}} = \bar{\mathbf{I}}_n [\mathbf{I}_n - \bar{\mathbf{I}}_n] w_k \tag{7}$$

The weighting function of the Kuan filter is defined as:

$$w_k = \frac{\sigma^2}{\sigma^2 + (\bar{\mathbf{I}}_n^2 + \sigma^2) / L} \tag{8}$$

### 2.1.2 Non-Linear Filtering Techniques

- **Median filter**

Median filtering is implemented by first arranging all pixels from the neighborhood into a numeral arrangement, and the median of these values is computed, and then the filtered pixels are replaced with the computed median [16].

- **Homomorphic Filter**

Generally, an image can be considered as a 2-D function.

$$\mathbf{I}(x, y) = \mathbf{R}(x, y) \cdot \mathbf{L}(x, y) \quad (9)$$

The product of illumination ( $\mathbf{L}$ ) and reflectance ( $\mathbf{R}$ ) results in intensity ( $\mathbf{I}$ ). Since illumination and reflectance are multiplicative components, they are turned into additive by applying the logarithm on the image intensity [17]. These components are separated linearly in the frequency domain. So, noise can be minimized by filtering in the log domain [18].

- **Speckle Reducing Anisotropic Diffusion (SRAD)**

In fact, it is shown that the SRAD [21,22] can be related directly to the Lee and Frost window-based filters. It reduces the noise via solving a partial differential equation (PDE) and identifying the edges. Given an image  $\mathbf{I}_0(x, y)$  over the 2-D coordinate grid  $\Omega$ , the output image  $\mathbf{I}(x, y; t)$  is evolved according to the following PDE:

$$\mathbf{I}(x, y; t) = \begin{cases} \frac{\partial \mathbf{I}(x, y; t)}{\partial t} = \text{div}[c(q) \nabla \mathbf{I}(x, y; t)] \\ \mathbf{I}(x, y; 0) = \mathbf{I}_0(x, y), \frac{\partial \mathbf{I}(x, y; t)}{\partial \vec{n}} \Big|_{\partial \Omega} = 0 \end{cases} \quad (10)$$

where  $\partial \Omega$  denotes the border of  $\Omega$ ,  $\vec{n}$  is the outer normal to the  $\Omega$  and  $c(q)$  is the diffusion coefficient.

- **Non-Local Means Filtering**

For the non-local means filter [23], the estimated value  $NL[v](i)$  for a pixel  $i$ , is computed as a weighted average of all the pixels in the image for a given discrete noisy image  $v = \{v(i) | i \in \mathbf{I}\}$ .

$$NL[v](i) = \sum_{j \in \mathbf{I}} w(i, j) v(j) \quad (11)$$

The filter weights can be represented as:

$$w(i, j) = \frac{1}{z(i)} e^{-\|v(N_i) - v(N_j)\|_{2,a}^2} \quad (12)$$

where  $z(i)$  is the normalizing constant.

- **Total Variation Minimization Algorithm**

It was presented in [24]. According to this principle, reducing the total variation of the noisy image makes it a close match to the ground truth image and removes the unwanted detail while preserving important details such as edges. It's mathematical given as follows:

$$TVF_\lambda(v) = \arg \min_u TV(u) + \lambda \int |v(x) - u(x)|^2 dx \quad (13)$$

where  $TV(u)$  denotes the total variation of  $u$  and  $\lambda$  is a given Lagrange multiplier.  $v(x)$  and  $u(x)$  are the original and noisy images.

## 2.2 Transform Domain-Based Noise Reduction Techniques

### 2.2.1 Wavelet Domain

- **Visu-Shrink**

Visu-shrink makes use of the global thresholding scheme. It adopts a hard threshold value  $T$  that is proportional to the standard noise deviation  $\sigma_n$  as follows [25]:

$$T = \sigma_n \sqrt{2 \log_{10} m} \quad (14)$$

where  $m$  is the image size.

- **Sure-Shrink**

Sure-shrink denoises an image by applying a soft threshold on the detail coefficients [25]. The objective of Sure shrink is to retain MSE as minimum as possible; it is defined as:

$$MSE = \frac{1}{n^2} \sum_{x,y=1}^n \left( \hat{\mathbf{I}}(x, y) - \mathbf{I}(x, y) \right)^2 \quad (15)$$

- **Wiener Filter**

Wiener filter belongs to a category of optimal linear filters. It gives a linear estimate of the image from its noisy version. Therefore, this filter needs information about the noise spectrum and the noise-free image [26].

- **Log Gabor Filter**

The transfer function of the Log-Gabor is given as [27]:

$$G(f) = e^{-\log(f/f_0)^2 / 2 \log(\sigma/f_0)^2} \quad (16)$$

where  $f_0$  is the center frequency of the filter and  $\sigma/f_0$  is the standard deviation of the Gaussian kernel.

The denoising procedure of the log-Gabor filter [27] is simple to implement and has the following steps:

- Multi-scale decomposition of the noisy image.
- Log-Gabor filtering of all sub-bands except for the approximation band.
- Soft thresholding of the filtered sub-bands.
- Inverse Discrete Wavelet Transform (DWT).

### 2.2.2 Curvelet Domain

- **Discrete Curvelet Transform Algorithm**

One of the weaknesses of the wavelet transform is that it is poor at extracting features from curves and edges of images, unlike curvelet transforms. The curvelet transform [28] is the development of the Ridgelet transform to identify arched borders efficiently.

## 2.3 Hybrid Noise Reduction Techniques

- **Combined Fourth-Order PDE and a Relaxed Median Filter Algorithm (Hybrid1)**

The hybrid filter combines the advantages of a fourth-order PDE and a comfortable intermediate filter [29] and is called the hybrid1 algorithm. Hybrid1 preserves subtle features, curved structures, sharp angles, and edges without compromising the features of the spatial neighborhood.

- **Combined Wavelet and Curvelet Transform Algorithm (Hybrid2)**

It is unsuitable for representing the high-level dimension singularities. On the other hand, the curvelet transform is used because it is robust when dealing with image edges, lines, and curves. So, combining both wavelet and curvelet transforms is superior to dealing with noisy images, unlike wavelet only or curvelet only.

### 3 Proposed Deep CNN-Based Medical Image Denoising Model

In the field of removing noise from images, deep learning structures have been presented for their high quality compared to traditional algorithms. This paper proposes deep learning models to reduce noise from medical images. Deep learning is characterized by its high efficiency; more data is used in the training phase. The proposed model for noise reduction consists of deep residual layers with BN. The remaining layers are distinguished by their ability to differentiate between real features and noise-generated features, and BN was used to achieve stability and speed up the training process. Our proposed model is considered a modification to the model in [32] research to make it suitable for reducing noise from medical images. The medical images differ from the rest of the images in the ambiguity of the features and the difficulty of perceiving them, like other digital images. The modification was done by adding deep residual layers and merging them with BN to improve performance and speed up the training process.

The proposed noise reduction model combines deep residual learning with BN, as shown in Fig. 2. It consists of three stages with different colors. 64 filters with size  $3 \times 3 \times 1$  are used and based on the training process, filter values are imposed. To reconstruct the output of the last layer, a single filter of size  $3 \times 3 \times 64$  is used. All pooling layers are removed. In order to optimize the proposed model and find the best values for the filters used, we used Stochastic Gradient Descent with Momentum (SGDM) with a mini-batch size of 128, a momentum of 0.9, and a weight decay of 0.0001.

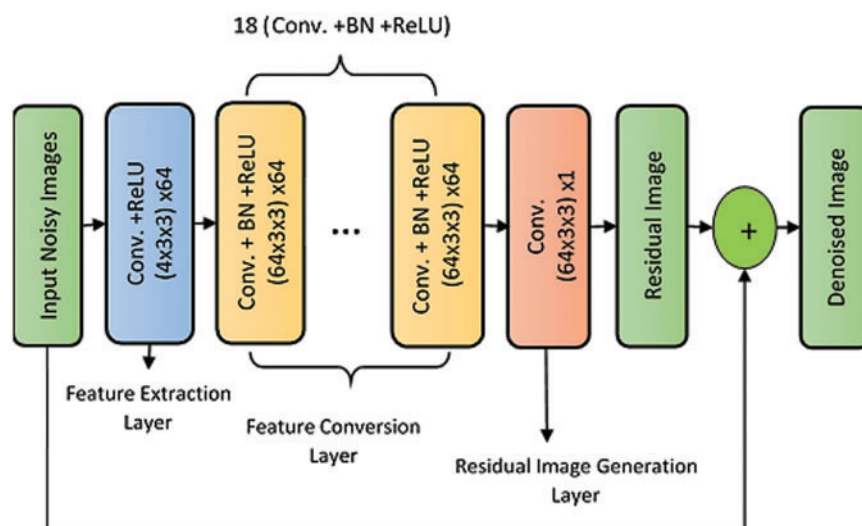


**Figure 2:** The proposed CNN-based denoising model

Without deep residual learning, the input density and the convolutional feature are correlated with neighboring ones. Without BN, the problem of internal variable transformation aggravates.

#### 4 Simulation Results and Discussions

Simulation results are presented using MATLAB R2019a on a Dell machine, Core i5 processor, 8 Gbytes RAMs, and 320 Gbytes hard disk. The metrics [31] used to measure the system performance are:

- **Peak Signal-to-Noise Ratio (PSNR) (dB)**

$$PSNR = 10 \log_{10} \frac{\max_{\mathbf{I}}^2}{MSE} \quad (17)$$

- **Correlation Coefficient ( $C_r$ )**

$$C_r = \frac{\sum_m \sum_n [(\mathbf{I}(m, n) - \bar{\mathbf{I}}) (\mathbf{I}_n(m, n) - \bar{\mathbf{I}}_n)]}{\sqrt{\left(\sum_m \sum_n (\mathbf{I}(m, n) - \bar{\mathbf{I}})^2\right) \left(\sum_m \sum_n (\mathbf{I}_n(m, n) - \bar{\mathbf{I}}_n)^2\right)}} \quad (18)$$

The higher the PSNR and  $C_r$  values of the image, the better the image quality.

- **Processing Time**

System complexity is expressed in terms of processing (CPU) time (seconds), which is calculated from the beginning of the simulation program to the end. The lower the CPU time of the image, the lower the algorithm complexity.

Five examples of scanned images were used. Also, different variances (0.2, 0.1, 0.05, 0.01) of speckle-noise are applied to simulate different scenarios. More than one type of filter has been applied to compare performance. Fig. 3 illustrates the performance of each algorithm applied to the Us image. The obtained PSNR and  $C_r$  values for each algorithm are calculated and tabulated for the Us image in Tab. 1. Gaussian noise was added to the other image modalities (X-ray, CT, PET, and MRI) with zero mean and different variances (0.01, 0.05, 0.1, and 0.2). To evaluate the subjective effect of these denoising methods, Figs. 4 to 7 show the performance of each algorithm applied on the X-ray, CT, PET, and MRI images, respectively. The obtained PSNR and  $C_r$  values for each algorithm are calculated and tabulated for each case in Tabs. 2 to 5, respectively.

Visual results of the Us breast image, shown in Fig. 3, reveal that the adaptive Lee, Kuan, and SRAD filters are superior to the other filtering techniques. They give the best image quality with preserved edges compared to Gaussian, Gabor, median, or log-Gabor. It is also apparent that the output of the denoising CNN outperforms most of the traditional denoising techniques. In addition, the visushrink and hybrid techniques have a smoothing effect.

From the presented results, the efficiency of the traditional filters is low when the noise level increases, as shown by the results of  $C_r$  and PSNR, respectively. On the contrary, the proposed CNN noise reduction model showed the best results at different speckle-noise levels, and it effectively reduces noise at the edges. The SRAD filter results in high results at lower noise levels on all the conventional filters. In Tab. 1, the suggested CNN model achieves the PSNR and  $C_r$  outcomes for all examined noise levels.

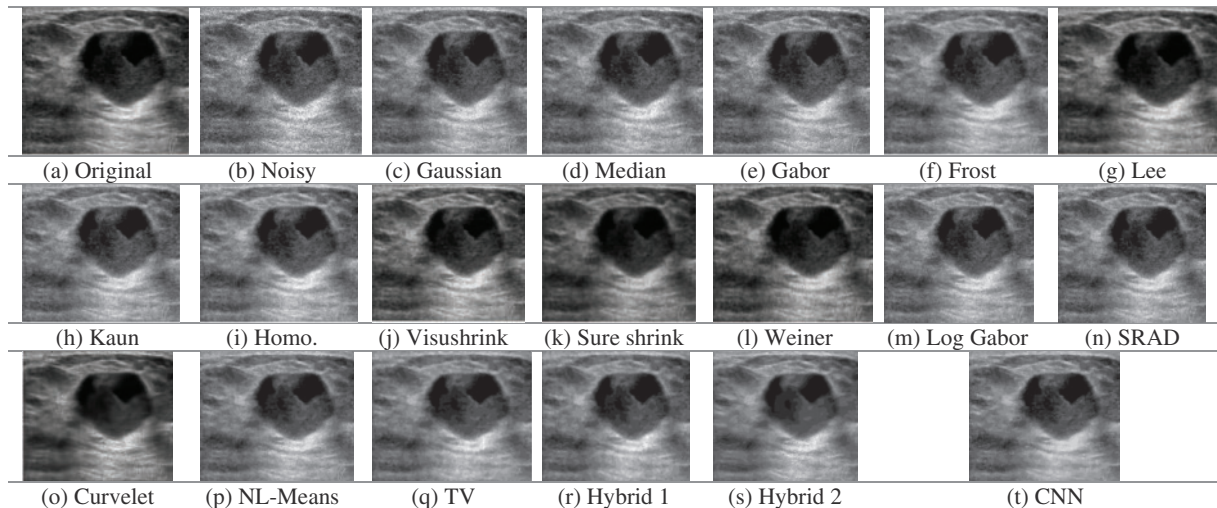


**Figure 3:** Obtained outcomes for the examined denoising filters for the US image at 0.05 speckle variance

**Table 1:** PSNR (dB) and  $C_r$  values for the Us image for speckle noise variance (0.01 to 0.2)

Technique	Speckle noise variance									
	0.01		0.03		0.05		0.1		0.2	
	PSNR	$C_r$	PSNR	$C_r$	PSNR	$C_r$	PSNR	$C_r$	PSNR	$C_r$
<b>Noisy Image</b>	28.0102	0.9769	23.2781	0.9353	21.0769	0.8985	18.1543	0.8233	15.2911	0.7128
<b>Gaussian</b>	31.5229	0.9895	27.0105	0.9707	24.8439	0.9527	21.9652	0.9116	19.0750	0.8436
<b>Median</b>	31.8548	0.9902	28.2434	0.9779	26.2418	0.9648	23.4612	0.9375	20.6344	0.8865
<b>Gabor</b>	30.7178	0.9872	26.1609	0.9642	24.1151	0.9436	21.3156	0.9003	18.8733	0.8378
<b>Lee</b>	31.0251	0.9936	30.2782	0.9884	29.7176	0.9829	28.3999	0.9698	25.9330	0.9435
<b>Frost</b>	33.6981	0.9890	31.0804	0.9873	29.4923	0.9853	26.8426	0.9799	24.2598	0.9677
<b>Kaun</b>	29.6997	0.9842	28.5180	0.9780	27.4657	0.9734	25.6790	0.9602	23.5323	0.9332
<b>Homomorphic</b>	31.8046	0.9932	29.9794	0.9875	28.5259	0.9815	25.8998	0.9657	23.0439	0.9279
<b>Visushrink</b>	31.2738	0.9884	29.8405	0.9844	28.7373	0.9811	27.3290	0.9734	25.5154	0.9563
<b>Sure shrink</b>	30.0209	0.9844	27.7644	0.9714	26.3253	0.9590	24.0820	0.9319	21.8351	0.8829
<b>Wiener</b>	30.7519	0.9872	27.7519	0.9745	26.0192	0.9629	23.3996	0.9359	20.8668	0.8861
<b>Log Gabor</b>	31.2268	0.9879	28.0981	0.9722	25.9501	0.9583	23.6430	0.9257	20.9773	0.8703
<b>SRAD</b>	33.7201	0.9943	30.2237	0.9872	27.0184	0.9734	22.4560	0.9283	18.3488	0.8308
<b>Curvelet</b>	31.1878	0.9885	28.8623	0.9796	27.8430	0.9736	26.3960	0.9631	24.4310	0.9447
<b>NL-Means</b>	31.4813	0.9894	29.6291	0.9834	26.8369	0.9680	22.1490	0.9142	17.8571	0.8068
<b>TV</b>	30.5038	0.9868	28.6299	0.9797	27.7866	0.9751	26.6413	0.9678	25.6245	0.9588
<b>Hybrid1</b>	29.5551	0.9836	28.6877	0.9800	28.1031	0.9770	26.8038	0.9688	25.1571	0.9544
<b>Hybrid2</b>	31.1325	0.9884	28.7915	0.9799	27.7608	0.9737	26.0562	0.9611	24.7046	0.9471
<b>CNN</b>	34.1454	0.9942	31.7398	0.9898	30.5050	0.9865	28.8336	0.9801	26.9512	0.9695

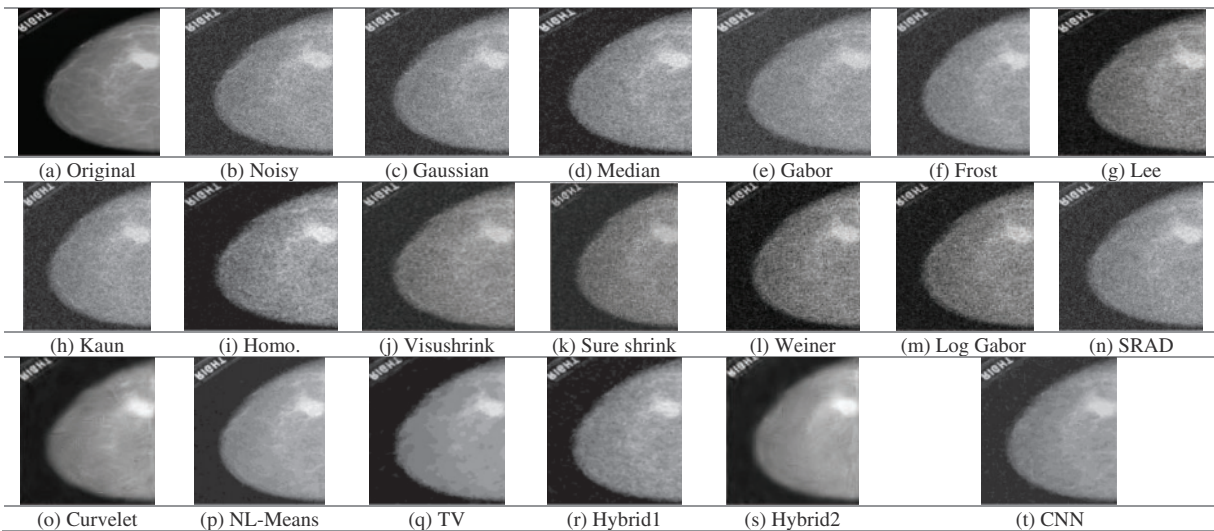


**Figure 4:** Obtained outcomes for the examined denoising filters for the XR image at 0.05 gaussian variance

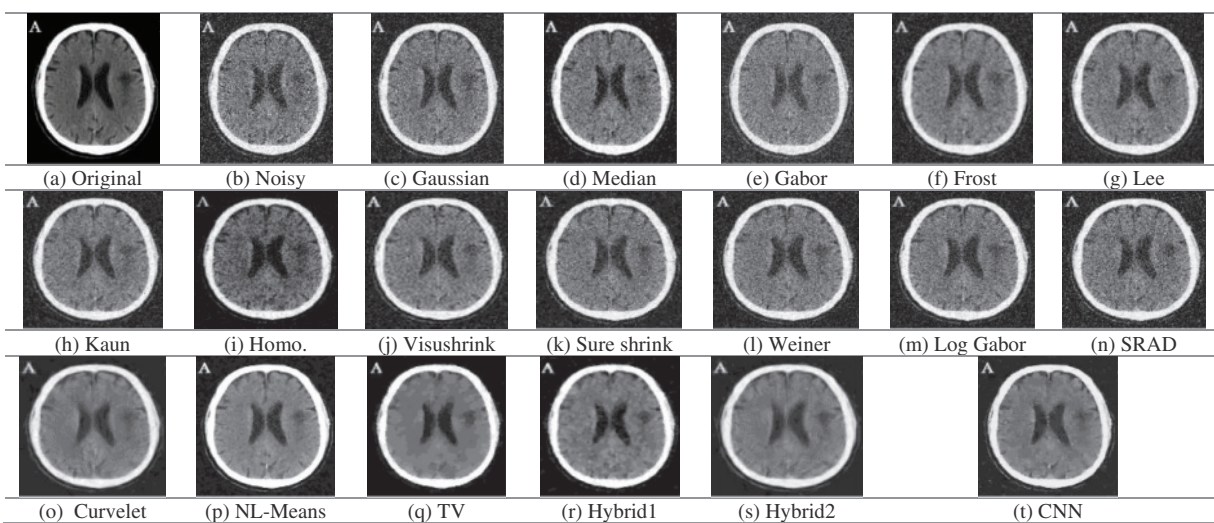


**Figure 5:** Obtained outcomes for the examined denoising filters for the CT image at 0.05 gaussian variance

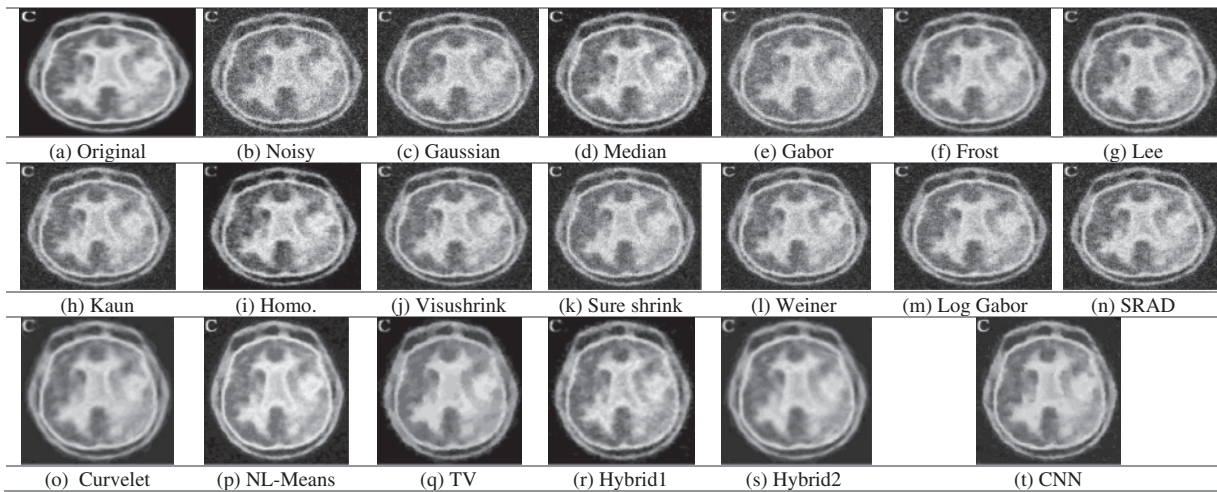


**Figure 6:** Obtained outcomes for the examined denoising filters for the PET image at 0.05 gaussian variance

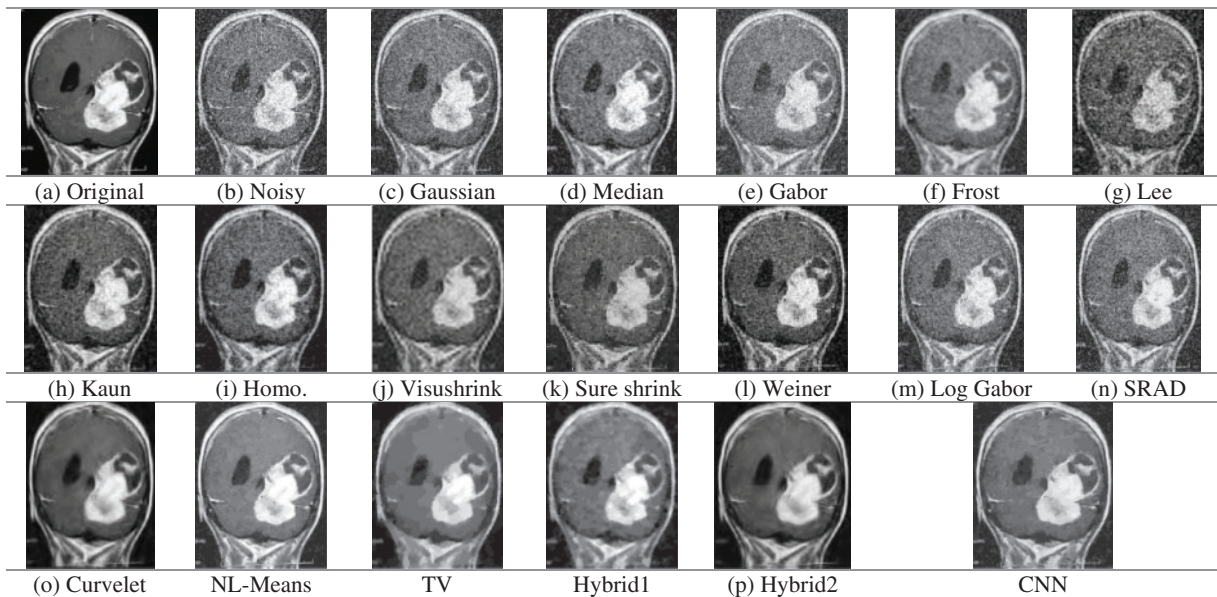


**Figure 7:** Obtained outcomes for the examined denoising filters for the MRI image at 0.05 gaussian variance

Fig. 4 depicts the visual results for the XR mammogram breast image. It is visible that most of the denoising techniques, including Gaussian, median, Gabor, Lee, Kuan, homomorphic, Wiener, Log-Gabor, and SRAD, failed to eliminate the Gaussian noise from the presented image. Visushrink, Curvelet, and hybrid two techniques decrease the resolutions of the image by more smoothing. The

best results are obtained from the TV, hybrid2, NL-Means filter, and the denoising CNN model, but more details are visualized from NL-Means and the denoising CNN model.

**Table 2:** PSNR (dB) and  $C_r$  values for the XR image for zero-mean Gaussian noise variance (0.01 to 0.2)

Technique	Gaussian noise variance									
	0.01		0.03		0.05		0.1		0.2	
	PSNR	$C_r$	PSNR	$C_r$	PSNR	$C_r$	PSNR	$C_r$	PSNR	$C_r$
<b>Noisy Image</b>	20.8417	0.9307	16.3059	0.8180	14.2466	0.7335	11.7785	0.5963	9.7049	0.4527
<b>Gaussian</b>	24.2116	0.9686	19.6733	0.9098	17.6424	0.8571	15.1068	0.7558	12.9636	0.6200
<b>Median</b>	27.4966	0.9856	23.5744	0.9617	21.4257	0.9380	18.6829	0.8865	15.7750	0.7942
<b>Gabor</b>	22.7385	0.9600	18.5825	0.8886	16.6564	0.8315	14.1818	0.7232	12.1790	0.5930
<b>Lee</b>	27.5990	0.9888	23.5932	0.9702	21.5189	0.9518	18.8085	0.9089	16.5610	0.8345
<b>Frost</b>	28.1974	0.9916	24.3441	0.9804	22.1030	0.9684	19.1931	0.9349	16.0889	0.8680
<b>Kaun</b>	25.6345	0.9811	23.0037	0.9623	21.0362	0.9447	18.7088	0.8999	16.4209	0.8253
<b>Homomorphic</b>	24.8801	0.9852	23.4499	0.9644	21.3680	0.9383	18.0231	0.8764	15.6528	0.7831
<b>Visushrink</b>	29.4553	0.9907	25.4594	0.9793	23.4119	0.9673	20.4498	0.9425	17.3240	0.8915
<b>Sure shrink</b>	27.7727	0.9823	23.4479	0.9472	21.0306	0.9133	18.6600	0.8438	16.8419	0.7400
<b>Wiener</b>	26.5541	0.9797	21.3295	0.9422	19.3624	0.9078	16.7756	0.8311	14.4832	0.7246
<b>Log Gabor</b>	26.6102	0.9798	21.6901	0.9420	19.6384	0.9051	16.8749	0.8315	14.6064	0.7172
<b>SRAD</b>	24.6479	0.9739	18.6893	0.8963	16.3092	0.8215	13.2565	0.6841	10.9619	0.5287
<b>Curvelet</b>	30.1469	0.9948	25.5695	0.9899	23.1681	0.9868	19.7396	0.9806	16.3888	0.9709
<b>NL-Means</b>	29.5036	0.9928	26.8895	0.9280	24.3828	0.8486	19.5614	0.6927	13.9213	0.5253
<b>TV</b>	32.9572	0.9956	31.0518	0.9931	29.6708	0.9905	27.9753	0.9859	26.5795	0.9805
<b>Hybrid1</b>	31.8790	0.9943	29.2743	0.9895	27.6129	0.9846	25.1477	0.9730	22.6010	0.9514
<b>Hybrid2</b>	29.9947	0.9947	25.6157	0.9905	22.8663	0.9867	19.6081	0.9799	16.3728	0.9719
<b>CNN</b>	31.5927	0.9959	27.2442	0.9922	24.8484	0.9875	21.4395	0.9723	18.0977	0.9238

**Table 3:** PSNR and  $C_r$  values for the CT image for zero-mean Gaussian noise variance (0.01 to 0.2)

Technique	Gaussian noise variance									
	0.01		0.03		0.05		0.1		0.2	
	PSNR	$C_r$	PSNR	$C_r$	PSNR	$C_r$	PSNR	$C_r$	PSNR	$C_r$
<b>Noisy Image</b>	21.2504	0.9610	16.6562	0.8887	14.6084	0.8264	12.0746	0.7097	9.8429	0.5654
<b>Gaussian</b>	24.3508	0.9825	19.8114	0.9477	17.7356	0.9142	15.1801	0.8410	12.8017	0.7259
<b>Median</b>	26.8152	0.9897	23.2161	0.9749	21.4063	0.9616	18.6989	0.9284	15.9557	0.8708
<b>Gabor</b>	22.6126	0.9768	18.5168	0.9356	16.5910	0.8992	14.0305	0.8179	11.7582	0.6908
<b>Lee</b>	25.7711	0.9898	22.4128	0.9795	20.6254	0.9680	18.1191	0.9413	15.5315	0.8901

(Continued)

**Table 3: Continued**

Technique	Gaussian noise variance									
	0.01		0.03		0.05		0.1		0.2	
	PSNR	$C_r$	PSNR	$C_r$	PSNR	$C_r$	PSNR	$C_r$	PSNR	$C_r$
<b>Frost</b>	24.6677	0.9875	22.1698	0.9806	20.5957	0.9732	18.0859	0.9517	15.4732	0.9050
<b>Kaun</b>	25.6804	0.9894	22.3472	0.9785	20.6589	0.9678	15.6298	0.9407	15.6298	0.8897
<b>Homomorphic</b>	24.7348	0.9855	21.7801	0.9725	19.7765	0.9580	17.2855	0.9295	15.1339	0.8853
<b>Visushrink</b>	25.7372	0.9846	23.0762	0.9759	21.4010	0.9690	19.3322	0.9536	16.8377	0.9213
<b>Sure shrink</b>	26.3055	0.9850	22.3146	0.9628	20.5255	0.9426	18.1173	0.8956	16.3270	0.8150
<b>Wiener</b>	24.9479	0.9781	20.5717	0.9540	18.6896	0.9326	16.2814	0.8856	13.9942	0.8025
<b>Log Gabor</b>	26.7553	0.9794	21.5293	0.9571	19.5878	0.9356	16.5129	0.8842	14.1402	0.7997
<b>SRAD</b>	24.0124	0.9820	18.7267	0.9338	16.3183	0.8843	13.5036	0.7800	11.0457	0.6388
<b>Curvelet</b>	26.9839	0.9922	23.2736	0.9859	21.4941	0.9818	18.6673	0.9750	15.8751	0.9663
<b>NL-Means</b>	26.8949	0.9925	25.5056	0.9579	23.7056	0.9098	19.6991	0.7945	14.3280	0.6450
<b>TV</b>	26.8886	0.9896	25.2115	0.9848	24.3905	0.9814	23.1479	0.9755	21.8237	0.9665
<b>Hybrid1</b>	26.3163	0.9881	25.0711	0.9843	24.2884	0.9814	22.7781	0.9734	20.8652	0.9579
<b>Hybrid2</b>	27.2471	0.9921	23.2134	0.9863	21.4237	0.9821	18.7692	0.9748	15.6992	0.9654
<b>CNN</b>	27.5218	0.9939	24.0469	0.9890	22.1856	0.9852	19.5071	0.9742	16.5437	0.9440

**Table 4: PSNR and  $C_r$  values for the PET image for zero-mean Gaussian noise variance (0.01 to 0.2)**

Technique	Gaussian noise variance									
	0.01		0.03		0.05		0.1		0.2	
	PSNR	$C_r$	PSNR	$C_r$	PSNR	$C_r$	PSNR	$C_r$	PSNR	$C_r$
<b>Noisy Image</b>	21.9919	0.9513	16.2779	0.8687	14.3088	0.8009	11.8568	0.6809	9.7758	0.5347
<b>Gaussian</b>	24.2541	0.9783	19.7425	0.9379	17.7246	0.9011	15.1753	0.8207	12.9744	0.6985
<b>Median</b>	27.5250	0.9894	23.2695	0.9721	21.3381	0.9571	18.5522	0.9178	15.7534	0.8547
<b>Gabor</b>	22.9991	0.9724	18.5260	0.9230	16.7427	0.8804	14.4317	0.7904	12.2406	0.6585
<b>Lee</b>	27.6146	0.9915	23.7542	0.9790	21.5806	0.9668	19.0184	0.9377	16.3794	0.8814
<b>Frost</b>	26.3703	0.9936	24.1481	0.9864	22.0482	0.9785	19.0347	0.9570	16.3938	0.9102
<b>Kaun</b>	27.7304	0.9917	23.5680	0.9792	21.7622	0.9675	19.0638	0.9368	16.4871	0.8815
<b>Homomorphic</b>	25.7552	0.9901	23.5884	0.9756	21.3679	0.9590	18.0643	0.9176	15.0424	0.8429
<b>Visushrink</b>	28.8860	0.9927	24.7521	0.9848	22.9498	0.9771	20.2938	0.9587	17.4668	0.9267
<b>Sure shrink</b>	26.3212	0.9842	22.3812	0.9605	20.7778	0.9372	18.5784	0.8885	16.7572	0.8021
<b>Wiener</b>	25.2018	0.9820	21.2506	0.9576	19.3351	0.9346	16.7560	0.8812	14.4884	0.7877
<b>Log Gabor</b>	27.8742	0.9829	22.1955	0.9579	19.8713	0.9326	17.0686	0.8793	14.7805	0.7866
<b>SRAD</b>	24.8477	0.9824	19.1599	0.9339	16.6160	0.8830	13.5993	0.7690	11.1118	0.6212
<b>Curvelet</b>	29.6287	0.9956	25.2134	0.9912	23.2785	0.9879	19.1151	0.9826	16.1441	0.9728
<b>NL-Means</b>	28.1281	0.9845	26.1022	0.9592	23.9174	0.9362	19.4972	0.8847	14.2592	0.8114
<b>TV</b>	28.7748	0.9923	26.5786	0.9872	25.3225	0.9828	23.9894	0.9767	22.4979	0.9665
<b>Hybrid1</b>	28.9717	0.9926	27.2100	0.9888	26.0103	0.9853	23.7560	0.9748	21.6449	0.9588

(Continued)

**Table 4:** Continued

Technique	Gaussian noise variance									
	0.01		0.03		0.05		0.1		0.2	
	PSNR	$C_r$	PSNR	$C_r$	PSNR	$C_r$	PSNR	$C_r$	PSNR	$C_r$
<b>Hybrid2</b>	29.8560	0.9956	25.0852	0.9913	23.8629	0.9883	19.3602	0.9826	16.4108	0.9733
<b>CNN</b>	29.4463	0.9948	25.8480	0.9900	23.7743	0.9862	20.7508	0.9746	17.6526	0.9402

**Table 5:** PSNR and  $C_r$  values for the MR image for zero-mean Gaussian noise variance (0.01 to 0.2)

Technique	Gaussian noise variance									
	0.01		0.03		0.05		0.1		0.2	
	PSNR	$C_r$	PSNR	$C_r$	PSNR	$C_r$	PSNR	$C_r$	PSNR	$C_r$
<b>Noisy Image</b>	20.6595	0.9418	16.1954	0.8458	14.2391	0.7743	11.7852	0.6445	9.7503	0.4978
<b>Gaussian</b>	24.0539	0.9721	19.7521	0.9237	17.7470	0.8802	15.2431	0.7896	13.0355	0.6590
<b>Median</b>	24.9326	0.9894	21.8559	0.9542	20.2686	0.9333	17.7958	0.8868	15.2203	0.8121
<b>Gabor</b>	22.8040	0.9643	18.7130	0.9083	16.9729	0.8592	14.4578	0.7593	12.3079	0.6278
<b>Lee</b>	25.1162	0.9800	22.5147	0.9647	20.9914	0.9485	18.7231	0.9098	16.4600	0.8445
<b>Frost</b>	22.9041	0.9696	21.5898	0.9614	20.5773	0.9518	18.5130	0.9238	16.2626	0.8694
<b>Kaun</b>	24.2906	0.9748	22.1072	0.9602	20.6297	0.9432	18.5023	0.9056	16.2856	0.8343
<b>Homomorphic</b>	23.3967	0.9726	20.5315	0.9533	18.7582	0.9353	16.3224	0.8987	14.2355	0.8303
<b>Visushrink</b>	23.9474	0.9644	21.8962	0.9474	21.0239	0.9346	18.9276	0.9112	17.1131	0.8720
<b>Sure shrink</b>	24.2459	0.9674	21.5347	0.9383	20.0618	0.9070	18.1824	0.8468	17.0809	0.7492
<b>Wiener</b>	22.9471	0.9384	20.0592	0.9077	18.6359	0.8830	16.3888	0.8241	14.3448	0.7280
<b>Log Gabor</b>	25.0336	0.9414	20.8461	0.9131	19.4042	0.8871	16.7860	0.8277	14.5672	0.7256
<b>SRAD</b>	23.7400	0.9724	18.5731	0.9092	16.1815	0.8463	13.4955	0.7289	11.1892	0.5755
<b>Curvelet</b>	27.2613	0.9877	23.8999	0.9785	22.1224	0.9716	19.4694	0.9603	16.1088	0.9426
<b>NL-Means</b>	27.1016	0.9778	25.5965	0.9457	23.6533	0.9162	19.4450	0.8544	14.1395	0.7703
<b>TV</b>	23.9425	0.9723	22.1255	0.9575	21.2340	0.9472	20.1232	0.9316	18.8790	0.9061
<b>Hybrid1</b>	22.5104	0.9609	21.6525	0.9522	21.0674	0.9445	20.0320	0.9284	18.8220	0.9040
<b>Hybrid2</b>	27.2223	0.9876	24.2374	0.9777	22.2588	0.9711	19.3878	0.9606	17.9452	0.9418
<b>CNN</b>	28.0531	0.9895	24.6735	0.9790	22.8408	0.9700	20.2205	0.9499	18.4544	0.9317

Tab. 2 shows the PSNR and  $C_r$  results for XR images using different variance levels for Gaussian noise. TV, NL-Means, hybrid1, and CNN techniques show higher PSNR scores than other technologies. But TV technique gives the highest results in PSNR and  $C_r$ . However, the small details are missed in the output images. The NL-Means filter shows high image recovery efficiency by improving edge and texture. This clarifies that NL-Means and CNN models have more advantages on XR mammogram breast image.

Fig. 5 shows the original, noisy, and output denoising results of the CT brain images. The traditional denoising techniques, including Gaussian, median, Gabor, Lee, Kuan, homomorphic,

wavelet-based, Log-Gabor, and SRAD techniques, poorly represented texture details, and poorly removed the Gaussian noise. On the other hand, the NL-Means filter and the denoising CNN model preserve edges and preserve texture details compared to the other techniques. [Tab. 3](#) shows the  $C_r$  and PSNR values for noisy and denoised images. We have found that the TV and hybrid1 techniques have the best PSNR output values. Indeed, they have the highest value of PSNR of 24.3905 dB (for TV) and 24.2884 dB (for hybrid 1) compared to 23.7056 dB (for NL-Means) and 22.1856 dB (for the denoising CNN) at 0.05 Gaussian noise variance. Through the presented results, we conclude that the NL-Means and CNN models show the best results and are considered the best models in reducing noise and preserving accurate features in CT brain images.

[Fig. 6](#) shows the outcomes of different noise reduction techniques of the PET brain images. According to the visualization, the Curvelet, hybrid2, TV, NL-Means, and CNN techniques eliminate the Gaussian noise efficiently. On the other hand, Gaussian, median, Gabor, Log-Gabor, and SRAD filters have a poor denoising performance. [Tab. 4](#) demonstrates the PSNR and  $C_r$  values for Gaussian noise variance of 0.01, 0.03, 0.05, 0.1, and 0.2. [Tab. 4](#) shows that the Curvelet, hybrid2, and CNN have the highest PSNR and  $C_r$  values at low noise variances. At high Gaussian noise variance, it is observed that the TV and hybrid1 techniques attain the best values for parameters PSNR and  $C_r$ . It appears from a perceptual and visual point of view that the Curvelet and the denoising CNN model restore edge and fine details more efficiently. Quantitatively, the TV and hybrid1 techniques have the best PSNR and  $C_r$  values.

[Fig. 7](#) shows the original, noisy, and denoised output images of the MRI brain images. The MRI image, shown in [Fig. 7a](#), has different regions, great details, smooth white, and dark regions with fine details. It is obviously shown in [Fig. 7b](#) that the noise severely degrades the image quality. Gaussian, median, Gabor, Lee, Weiner, Log-Gabor, and SRAD filters poorly deal with the image noise, and residual noise and the artifacts still exist. Wavelet-based techniques, visushrink, and sure shrink, smooth the image and affect the contrast heavily. Moreover, the Frost, Curvelet, and hybrid2 output results are blurred seriously. [Fig. 7](#) shows the perceptual and visual superiority of the NL-Means and CNN models over the rest of the models.

The CNN model for Gaussian noise reduction excels from the MRI image in [Tab. 5](#). The  $C_r$  values of hybrid2 and the CNN model are higher than hybrid1 and the TV techniques with lower  $C_r$  values. It is noticed that the CNN model is more efficient to denoise multimodal medical images with different noise types at low, medium, and high noise variances. As a result of using deep residual learning, the proposed model outperformed CNN by separating noise from noisy images.

[Tab. 6](#) presents the CPU time for all the previously mentioned noise reduction techniques for the different image modalities. In the case of the Us image, models took much time to process because the Us image is the highest compared to the other image modalities due to the image size and the scan type. Due to the use of local statistics, the Lee filter outperforms adaptive filters based on wavelet and hybrid techniques in terms of processing speed. The Curvelet-based techniques have the highest processing time compared to the other techniques, up to 34 s for the Us image and 25 s for the other modalities. These techniques spend much more time because of the several transforms applied to the image before denoising. The denoising CNN model gives the most satisfying denoising results at a good CPU time, and it can also be considered an online processing model.

**Table 6:** The CPU time for the different image modalities

Technique	Image processing CPU time (s)				
	Us	XR	CT	PET	MR
<b>Gaussian</b>	0.05	0.03	0.03	0.03	0.03
<b>Median</b>	0.16	0.05	0.06	0.05	0.06
<b>Gabor</b>	1.2	0.7	0.68	0.7	0.65
<b>Lee</b>	0.03	0.02	0.02	0.02	0.02
<b>Frost</b>	6.9	3.4	3.4	3.4	3.5
<b>Kaun</b>	12.3	9.3	8.9	9.1	8.9
<b>Homomorphic</b>	0.14	0.13	0.12	0.11	0.12
<b>Visushrink</b>	0.56	0.13	0.12	0.11	0.11
<b>Sure shrink</b>	0.12	0.11	0.09	0.09	0.12
<b>Wiener</b>	1.6	0.5	0.5	0.4	0.5
<b>Log Gabor</b>	0.69	0.3	0.2	0.3	0.3
<b>SRAD</b>	13.3	7.3	7.1	7.1	6.9
<b>Curvelet</b>	33.4	23.3	23.8	23.5	23.2
<b>NL-Means</b>	6.4	3.4	1.92	1.41	1.03
<b>TV</b>	8.3	7.4	3.2	4.4	1.9
<b>Hybrid1</b>	19.7	17.5	8.2	7.8	6.7
<b>Hybrid2</b>	34.1	25.4	25.1	25.6	25.3
<b>CNN</b>	7.07	4.58	4.03	4.45	2.78

### • Results Discussion

The obtained results demonstrate that the Gaussian and Gabor filters cannot remove Speckle or Gaussian noise, especially with large noise variances. The Gaussian filter also smoothes images and blurs the edges. The median filter is more robust than the Gaussian filter because it preserves edges. The Lee filter has a smoothing effect if the area has low variance. However, it fails to remove noise from areas closer to edges and lines. The Frost filter relies on adaptive filtering between pixels to reduce noise and smoothes the homogeneous regions. The Kuan filter has the advantage of preserving sharp edges compared to Frost and Lee filters. However, it is not effective at high noise variances.

The Homomorphic filter can maintain the brightness of images and increase the contrast. In the SRAD model, its performance decreases with increasing noise variance. However, it can remove speckle noise while maintaining edge features. In investigating various image denoising methods based on wavelet transform, it has been found that the sub-band adaptive thresholding methods outperformed the highest spatial domain method in the MRI image for all noise levels. If they did not perform better, they were slightly better than the Gaussian and Gabor filters. Out of the sub-band adaptive methods, sure-shrink consistently outperformed and visushrink. Because sure-shrink filtering is adaptive when dealing with images that contain abrupt changes or boundaries.

On the other hand, visushrink removes too many coefficients and overly smooths images. Wiener filter yields better results when the image is corrupted with a Gaussian noise rather than speckle

noise. The Log-Gabor filter is poor when dealing with noisy images. The curvelet denoising technique is suitable when dealing with image edges and curves. The NL-mean filter is characterized by its ability to preserve the clarity of images and less information loss, especially at low noise variance. This is the result of taking the average of all pixels in the image as opposed to local mean filtering. The TV algorithms have advantages such as mean filtering and linear dimming that preserve edge characteristics and reduce noise in flat areas, at most high and low noise variances.

Hybrid algorithms are characterized by combining the features of discrete algorithms such as Hybrid Model 1, which outperforms other algorithms in terms of edges and structures. Hybrid Model 2 was also implemented by combining wavelet and curve transformation models. The curvelet transform model is characterized by representing curves in the images, and the wavelet transform model is characterized by reducing noise in smooth areas. One of the problems with the Hybrid Model 2 is that it takes a longer time to process. However, it significantly outperforms wavelet-based technologies.

In contrast to traditional noise reduction techniques, the CNN noise reduction model can handle noisy images with different noise levels. It also reduces quantitative and qualitative noise. The CNN model is characterized by its ability to adapt in all modalities of medical images, unlike other models that excel in some modalities and fail in other modalities of images. Moreover, visual comparisons of the different algorithms show that the CNN noise reduction model produces more perceptive images with sharp edges and finer information.

## 5 Conclusions and Future Work

This paper presented a CNN-based denoising model and a comparative study of noise reduction methods for various medical image modalities. The performance of all employed methods is tested on different medical images (Us, X-ray, CT, PET, and MR). This study can summarize all the noticed advantages and disadvantages of the tested noise reduction techniques employed in this paper on different medical image modalities. The employed algorithms are tested on the medical images, and their denoising performance has been compared and studied. For the spatial domain, median filtering outperformed the Gaussian filtering. The superiority of the waveform model in reducing Gaussian noise was proven to be significantly superior to the rest of the other models. It has shown the best image quality. From comparing the denoising results of different denoising techniques using different threshold functions, it is obvious that the images become blurred after global threshold denoising. On the other hand, the image texture details are well preserved using the wavelet denoising method based on adaptive thresholding. The comparison is more obvious in the MRI image, which has more texture details. Similar results can be obtained for other test images. The curvelet algorithms excel at reducing noise in some image modalities such as curvilinear images and linear singularities. Moreover, the hybrid algorithm based on combining wavelet and curvelet transforms maximizes the advantages of both. The numerical and visual results show that the proposed CNN noise reduction model is adapted to all modalities of medical images in terms of perceptual and visual quality. It also possesses high scores in most noise levels and image modalities. Therefore, we conclude that the CNN model is superior to traditional filtering and noise reduction techniques. The CNN model also has a good denoising CPU time. For future work, combinations of other transforms and the adaptation of CNN models could yield better results than those obtained separately.

**Acknowledgement:** Princess Nourah bint Abdulrahman University Researchers Supporting Project number (PNURSP2022R66), Princess Nourah bint Abdulrahman University, Riyadh, Saudi Arabia.

**Funding Statement:** Princess Nourah bint Abdulrahman University Researchers Supporting Project number (PNURSP2022R66), Princess Nourah bint Abdulrahman University, Riyadh, Saudi Arabia.

**Conflicts of Interest:** The authors declare that they have no conflicts of interest to report regarding the present study.

## References

- [1] W. El-Shafai, "Joint adaptive pre-processing resilience and post-processing concealment schemes for 3D video transmission," *3D Research*, vol. 6, no. 1, pp. 1–21, 2015.
- [2] W. El-Shafai, S. El-Rabaie, M. El-Halawany and F. Abd El-Samie, "Encoder-independent decoder-dependent depth-assisted error concealment algorithm for wireless 3D video communication," *Multimedia Tools and Applications*, vol. 77, no. 11, pp. 13145–13172, 2018.
- [3] M. Diwakar and M. Kumar, "A review on CT image noise and its denoising," *Biomedical Signal Processing Control*, vol. 42, no. 5, pp. 73–88, 2018.
- [4] W. El-Shafai, S. El-Rabaie, M. El-Halawany and F. Abd El-Samie, "Enhancement of wireless 3D video communication using color-plus-depth error restoration algorithms and Bayesian Kalman filtering," *Wireless Personal Communications*, vol. 97, no. 1, pp. 245–268, 2017.
- [5] W. El-Shafai, S. El-Rabaie, M. El-Halawany and F. Abd El-Samie, "Recursive Bayesian filtering-based error concealment scheme for 3D video communication over severely lossy wireless channels," *Circuits Systems, and Signal Processing*, vol. 37, no. 11, pp. 4810–4841, 2018.
- [6] H. El-Hoseny, W. El-Rahman, W. El-Shafai, S. M. El-Rabaie, K. Mahmoud *et al.*, "Optimal multi-scale geometric fusion based on non-subsampled contourlet transform and modified central force optimization," *International Journal of Imaging Systems and Technology*, vol. 29, no. 1, pp. 4–18, 2019.
- [7] B. Goyal, A. Dogra, S. Agrawal and B. Sohi, "Noise issues prevailing in various types of medical images," *Biomedical & Pharmacology Journal*, vol. 11, no. 3, pp. 1227–1237, 2018.
- [8] L. Fan, F. Zhang and H. Fan, "Brief review of image denoising techniques," *Visual Computing for Industry, Biomedicine, and Art*, vol. 2, no. 7, pp. 1–12, 2019.
- [9] B. Goyal, A. Dogra, S. Agrawal, B. Sohi and A. Sharma, "Image denoising review: From classical to state-of-the-art models," *Information Fusion*, vol. 55, no. 7, pp. 220–244, 2020.
- [10] S. Garg, R. Vijay and S. Urooj, "Statistical model to compare image denoising techniques in medical MR images," *Procedia Computer Science*, vol. 152, no. 3, pp. 367–374, 2019.
- [11] A. Sedik, H. Emara, A. Hamad, E. Shahin, N. El-Hag *et al.*, "Efficient anomaly detection from medical signals and images," *International Journal of Speech Technology*, vol. 22, no. 3, pp. 739–767, 2019.
- [12] S. Singh and I. Singula, "Enhanced face matching technique-based Gabor Filter and PSO," *International Journal of Advanced Research in Computer Science and Software Engineering*, vol. 4, no. 8, pp. 1215–1220, 2014.
- [13] W. El-Shafai, S. El-Rabaie, M. El-Halawany and F. Abd El-Samie, "Proposed dynamic error control techniques for QoS improvement of wireless 3D video transmission," *International Journal of Communication Systems*, vol. 31, no. 10, pp. 1–23, 2018.
- [14] W. El-Shafai, S. El-Rabaie, M. El-Halawany and F. Abd El-Samie, "Proposed adaptive joint error-resilience concealment algorithms for efficient colour-plus-depth 3D video transmission," *IET Image Processing*, vol. 12, no. 6, pp. 967–984, 2018.
- [15] A. Chaari, K. Kammoun, I. Kallel, M. Frikha and J. Feki, "Performance evaluation of various denoising filters and segmentation methods for OCT images," in *Proc. 5th Int. Conf. on Advanced Technologies for Signal and Image Processing (ATSIP)*, Sousse, Tunisia, pp. 1–6, 2020.
- [16] B. Ahamed, D. Yuvaraj and S. Priya, "Image denoising with linear and non-linear filters," in *Proc. Int. Conf. on Computational Intelligence and Knowledge Economy (ICCIKE)*, Dubai, United Arab Emirates, pp. 806–810, 2019.

- [17] W. El-Shafai, S. El-Rabaie, M. El-Halawany and F. Abd El-Samie, "Performance evaluation of enhanced error correction algorithms for efficient wireless 3D video communication systems," *International Journal of Communication Systems*, vol. 31, no. 1, pp. 1–27, 2018.
- [18] A. Odat, M. Otair and F. Shehadeh, "Image denoising by comprehensive median filter," *International Journal of Applied Engineering Research*, vol. 10, no. 15, pp. 36016–36022, 2015.
- [19] S. Orcioni, A. Paffi, F. Camera, F. Apollonio and M. Liberti, "Automatic decoding of input sinusoidal signal in a neuron model: High pass homomorphic filtering," *Neurocomputing*, vol. 292, no. 2, pp. 165–173, 2018.
- [20] H. El-Hoseny, W. Abd El-Rahman, W. El-Shafai, G. El-Banby, E. El-Rabaie *et al.*, "Efficient multi-scale non-sub-sampled shearlet fusion system based on modified central force optimization and contrast enhancement," *Infrared Physics & Technology*, vol. 10, no. 2, pp. 102–123, 2019.
- [21] H. Hammam, W. El-Shafai, E. Hassan, A. El-Azm, M. Dessouky *et al.*, "Blind signal separation with noise reduction for efficient speaker identification," *International Journal of Speech Technology*, vol. 4, no. 6, pp. 1–16, 2021.
- [22] N. El-Hag, A. Sedik, W. El-Shafai, H. El-Hoseny, A. Khalaf *et al.*, "Classification of retinal images based on convolutional neural network," *Microscopy Research and Technique*, vol. 84, no. 3, pp. 394–414, 2021.
- [23] A. Mahmoud, W. El-Shafai, T. Taha, E. El-Rabaie, O. Zahran *et al.*, "A statistical framework for breast tumor classification from ultrasonic images," *Multimedia Tools and Applications*, vol. 80, no. 4, pp. 5977–5996, 2021.
- [24] W. El-Shafai, E. El-Rabaie, M. Elhalawany and F. Abd El-Samie, "Improved joint algorithms for reliable wireless transmission of 3D color-plus-depth multi-view video," *Multimedia Tools and Applications*, vol. 78, no. 8, pp. 9845–9875, 2019.
- [25] Y. Zhan, W. Ding and F. Pan, "Improved wavelet threshold for image de-noising," *Frontiers in Neuroscience*, vol. 13, no. 1, pp. 1–39, 2019.
- [26] V. Strela, "Denoising via block wiener filtering in wavelet domain," in *Proc. IEEE 3rd European Congress of Mathematics*, Barcelona, Birkhäuser Verlag, pp. 619–625, 2001.
- [27] W. El-Shafai, S. El-Rabaie, M. El-Halawany and F. Abd El-Samie, "Efficient hybrid watermarking schemes for robust and secure 3D-MVC communication," *International Journal of Communication Systems*, vol. 31, no. 4, pp. 1–22, 2018.
- [28] K. Abdelwahab, S. Abd El-atty, W. El-Shafai, S. El-Rabaie and F. Abd El-Samie, "Efficient SVD-based audio watermarking technique in FRT domain," *Multimedia Tools and Applications*, vol. 79, no. 9, pp. 5617–5648, 2020.
- [29] J. Rajan, K. Kannan and M. Kaimal, "An improved hybrid model for molecular image denoising," *Journal of Mathematical Imaging and Vision*, vol. 31, no. 3, pp. 73–79, 2008.
- [30] A. Mahmoud, S. Rabaie, T. Taha and F. Abd El-Samie, "Mixed curvelet and wavelet transforms for speckle noise reduction in ultrasonic b-mode images," *Information Sciences and Computing*, vol. 3, no. 9, pp. 1–21, 2015.
- [31] O. Faragallah, A. Afifi, W. El-Shafai, H. El-Sayed, E. Naeem *et al.*, "Investigation of chaotic image encryption in spatial and FrFT domains for cybersecurity applications," *IEEE Access*, vol. 8, pp. 42491–42503, 2020.
- [32] K. Zhang, W. Zuo, Y. Chen, D. Meng and L. Zhang, "Beyond a gaussian denoiser: Residual learning of deep CNN for image denoising," *IEEE Transactions on Image Processing*, vol. 26, no. 7, pp. 3142–3155, 2017.